 DOI: 10.1002/maco.201307533

Study of polymer coating delamination kinetics on zinc modified with zinc oxide of different morphologies

Dedicated to Professor Dr. Martin Stratmann on the occasion of his 60th birthday.

D. Iqbal, R. Singh Moirangthem†, A. Bashir and A. Erbe*

Industrially prepared materials surfaces often possess complex morphologies and topographies. Using rough model interfaces, the effect of the surface morphology on the delamination of a polymer coating from zinc surfaces is investigated in this work. Zinc oxide particles of different shapes with characteristic dimensions ~1 µm were deposited on zinc surfaces to serve as model corrosion products with well-defined morphologies. Surfaces with spherical, rod-shaped, and twin-plate-shaped zinc oxide particles were prepared and characterized by scanning electron microscopy (SEM) as well as X-ray diffraction (XRD). The surfaces were subsequently coated with poly(vinyl butyral) (PVB) as a model for a weakly bound polymer coating. Scanning Kelvin probe (SKP) measurements were carried out in humid air to study the delamination kinetics. Results were compared to PVB on zinc. While delamination is fastest on zinc without zinc oxide particles, the delamination rate on the particle-covered surfaces strongly depends on the particle morphology. Delamination rate increases in the order sphere < rod < twin-plate, with differences by one order of magnitude between fastest and slowest. The differences in delamination rate can be understood based on the surface energies of the terminating surfaces of the particles, and the resulting differences in stability under conditions of zinc oxide dissolution.

1 Introduction

A number of modern and traditional methods exist to protect reactive structural materials, such as steels, against corrosion [1–10]. Zinc is extensively used as a protective metallic coating for steels. The intense use of zinc as a protective coating for steels stems from its excellent corrosion protection properties in air and other environments [11]. Bare zinc may be coated with polymers to provide a barrier against aqueous electrolytes and oxygen, which are responsible for corrosion processes [7,12,13]. However, due to presence of defects and free volume in polymer coatings, electrochemical reactions occur at polymer/metal interface in the presence of water as well as humid atmosphere, which lead to corrosion of metal [14]. The most important mechanism for the failure of organic coatings on bare zinc is cathodic delamination, where, through the formation of a galvanic cell, metal dissolves actively at a local anode in a defect area, while oxygen reduction occurs at a local cathode within delaminated region. The resulting potential difference leads to progression of a delamination front under the coating [15].

Zinc is always covered with a thin oxide layer, which determines its adhesion to the polymer [16–18], which is related to its resistance against corrosion. Previous studies have shown that interfacial oxide chemistry plays an important role in adhesion between polymer/metal interfaces. In particular, tailoring the hydroxyl/oxide ratio could lead to the enhancement in the adhesion at polymer/oxide/metal interface [19]. The native oxide differs in its electronic structure substantially from the crystalline oxide, especially due to the presence of intragap states, which may affect adhesion properties [20,21]. Naturally, the thickness of the oxide films depends on the electrochemical polarization and atmospheric conditions [22,23]. The dissolution kinetics of zinc oxide under the conditions of cathodic delamination may, however, also be a crucial factor when determining the rate of delamination.

D. Iqbal, R. Singh Moirangthem, A. Bashir, A. Erbe
Department of Interface Chemistry and Surface Engineering, Max-Planck-Institut für Eisenforschung GmbH, Max-Planck-Str. 1, 40237 Düsseldorf, (Germany)
E-mail: a.erbe@mpie.de

†Current address: Department of Applied Physics, Indian School of Mines, Dhanbad 826004, Jharkhand (India).

Zinc oxide itself has become an interesting functional material in a number of areas, e.g., for application in LEDs [24], solar cells [25], catalysis [26], and nano-sensing [27]. For most of these applications, micro- or nanostructured surfaces, or small particles are used, where "small" refers to size parameters below 10 µm. The properties of micro- and nanostructured zinc oxide can be affected via control of size and shape [28,29]. Therefore, a variety of different crystal shapes has been synthesized, ranging from rods/tubes [30], belts [31], spheres [32], to more complex ones like urchins [33], flowers [34], twin-plates [35], and pine trees [36].

In corrosion protection, the formation of a layer of protective corrosion products on a surface is crucial [37–39]. By deposition of artificial corrosion products on the surface of steel and galvanized steel, the effect of oxides on the oxygen reduction was recently investigated [39]. This work follows a similar idea: zinc oxide particles with different shapes are deposited on zinc surfaces, and delamination of a model polymer coating is investigated. Zinc oxide crystals of different sizes and shapes (determining overall surface morphology) exhibit different stability towards wet etching in a basic medium, as occurs during cathodic delamination. Zinc oxide dissolution in an alkaline medium has shown to take place at crystal edges [40]. Consequently, the rate of delamination of a polymer coating should be affected by the oxide surface on top of the zinc coating. A test of this hypothesis is subject of this work. Therefore, spherical, rod-shaped, and twin-plate-shaped zinc oxide particles have been synthesized via a sol–gel route, and deposited on a metallic zinc substrate. Subsequently, poly(vinyl butyral) (PVB) coatings, as a model for weakly bound polymers on the zinc, have been deposited, and the delamination kinetics was studied in a humid air atmosphere by scanning Kelvin probe (SKP) measurements.

2 Experimental

2.1 Materials

Poly(vinyl butyral), absolute ethanol, KCl, and all chemicals needed for the particle synthesis ($Zn(NO_3)_2 \cdot 6H_2O$, hexamethylenetetramine, gelatin, trisodium citrate) were obtained from Sigma–Aldrich and were used as received. Zinc sheets (purity, 99.95%) having a thickness of 1.5 mm were obtained from Goodfellow (Cambridge, UK) and cut to a size of $20 \times 15\ mm^2$. Zinc sheets were initially mechanically ground up to 4000 grit using SiC paper, followed by polishing with diamond paste of 1 µm size. Subsequently, the polished zinc substrates were cleaned with acetone/water and dried in nitrogen stream.

2.2 Synthesis of zinc oxide modified surfaces

A solution containing zinc nitrate hexahydrate [$Zn(NO_3)2 \cdot 6H_2O$] and hexamethylenetetramine (HMT) was prepared in ultrapure water, containing each at a concentration of 50 mM. The solution was stirred at room temperature with a magnetic stirrer at 1200 rpm until a clear solution was obtained (~10 min). For the synthesis of rod-like zinc oxide, the obtained solutions were directly heated (see below) without any capping agent. For the synthesis of twin-plate-shaped zinc oxide, gelatin was dissolved in the obtained solution with a concentration of 5 g/L. For the synthesis of spherical zinc oxide particles, a 40 mM solution of trisodium citrate ($Na_3C_6H_5O_7$) in ultrapure water is mixed with the double volume of $ZnNO_3$/HMT solution in a glass beaker.

Next, a clean polished zinc sheet substrate was put into the respective solution in a glass vial. The vial was tightly closed and then placed inside an oven for 90 min at a temperature of 90 °C. After letting the solution cool down to room temperature, the modified zinc substrates were removed from the solution and washed several times with water and then with ethanol to remove contaminants. Finally, the samples were dried in a nitrogen stream and kept in a desiccator until used.

2.3 Scanning Kelvin probe delamination studies

Initially, zinc oxide-particle modified zinc substrates and bare zinc substrates were spin coated with 5 wt% PVB dissolved in ethanol and dried in an oven at 70 °C for 1 h. A coating with a thickness of ~1 µm was obtained under these conditions. In order to initiate the cathodic delamination process, an artificial defect was created at the edge of the sample with a scalpel, and the defect was filled with 10 µL of 3 M KCl. The samples were subsequently introduced into humid SKP chamber at 92–95% relative humidity at a temperature around 23 °C. Delamination experiments were performed on a commercial SKP system from KM Soft Control (Wicinski – Wicinski GbR, Wuppertal, Germany) with a 100 µm NiCr tip. Before each experiment, the Kelvin probe was calibrated to the standard hydrogen electrode (SHE) against a $Cu/CuSO_4$ reference electrode. The progress of cathodic delamination has been analyzed according to the procedure described in Ref. [14].

2.4 Characterization methods

The surface morphology of zinc oxide-particle modified zinc was examined by scanning electron microscopy (SEM, Zeiss LEO 1550 VP). Crystallographic information about the reaction products was obtained by X-ray diffraction (XRD, Bruker-AXS D8 with a Cu K_α source) in grazing incidence geometry at an angle of incidence of 3 ° for minimizing the substrate diffraction, and enhancing the diffraction from the zinc oxide layer. For peak identification in the diffraction patterns, the Diffrac Plus database JCPDS was used. In this work, powder diffraction file nos. 03-065-3358 and 00-005-0664 were compared against the measured diffraction patterns.

3 Results and discussion

Different microstructures with a certain distribution in size and diameter of the zinc oxide particles were grown on polished zinc sheet using the hydrothermal technique described above. Figure 1 shows the SEM images of twin-plate-shaped (a), rod-shaped (b), and spherical (c) zinc oxide microstructures precipitated on the zinc sheet substrate. Rod-like structures were synthesized without any surface capping agent, due to the tendency of *c*-axis growth of zinc oxide [41].

To obtain other morphologies of zinc oxide, gelatin and sodium citrate were used for selective protection of one surface.

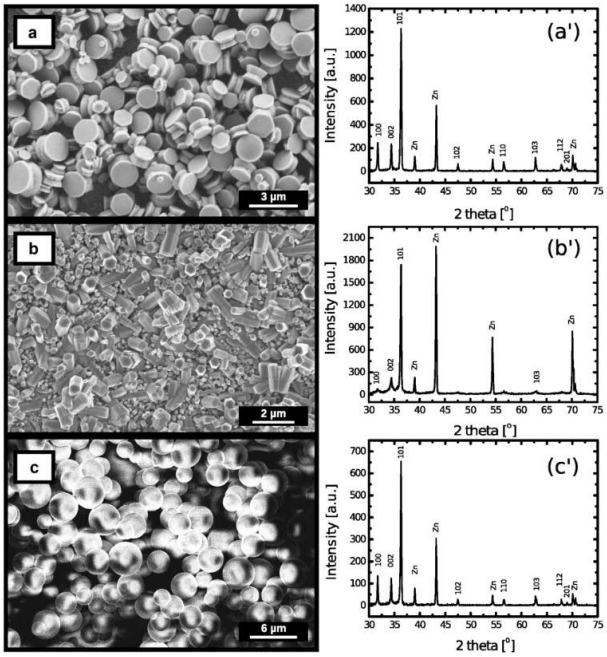

Figure 1. SEM micrographs and XRD patterns of grown ZnO structures on metallic zinc. Left panel: SEM images of (a) ZnO twin plates, (b) ZnO rods, and (c) ZnO spheres. Right panel: XRD patterns of (a′) ZnO twin plates, (b′) ZnO rods, and (c′) ZnO spheres

The detailed growth mechanism of twin-plate-shaped zinc oxide has been discussed in Refs. [35,42], while the respective mechanism for growth of spherical particles is described in Refs. [43,44]. By varying the growth time and concentration of the surface protecting agents, the size and morphology of the zinc oxide microstructure can easily be varied.

XRD data, also shown in Fig. 1, confirms the crystalline nature of the produced zinc oxide particle-covered surfaces. Comparing the relative intensity ratios of the different zinc oxide peaks to powder diffraction file no. 00-005-0664 for zinc oxide shows slight deviations. The most prominent peak is in all cases the 101 peak, though its intensity compared to other peaks in all patterns in this work is higher than in the reference data. On the other hand, the second most intense {100} peak from the reference data is less prominent in the data obtained here. While the patterns for spheres and twin-plates are quite similar, the rod's pattern shows only a small intensity of the {100} peak, but a substantial {002} peak. While there clearly is some preferential growth direction, the overall deviations from the powder data does not indicate a strong dominance of one direction, as would be expected for *c*-axis growth on surfaces [41]. While there is some evidence for *c*-axis growth in the rod-shaped particles, it is in all cases the patterns are dominated by the {101} peak, belonging to one of the stable non-polar surfaces of zinc oxide [41,45]. Figure 2 shows averaged SKP potential scans of the delamination experiments of PVB coatings on zinc and zinc modified with zinc oxide of different morphologies. Initially, SKP measures a potential of the intact polymer/oxide/metal interface. However with time, cathodic delamination is initiated in a humid air atmosphere on all the samples, as can be seen in Fig. 2 by two distinct potential levels [14]. A more negative potential ($\sim -0.7\,V_{SHE}$) indicates actively corroding metal surface at the defect/delaminated region, while more positive potentials ($\sim -0.2\,V_{SHE}$) demonstrate intact polymer/oxide/metal interface [14]. Between these two potentials, a very sharp potential jump can be observed, which characterizes the delamination front, a transition between intact coating and delaminated interface [14]. The progress of the delamination front with time is plotted in Fig. 3 for three representative examples from each surface morphology, and the slope of a linear fit was determined. This slope is discussed as delamination velocity below.

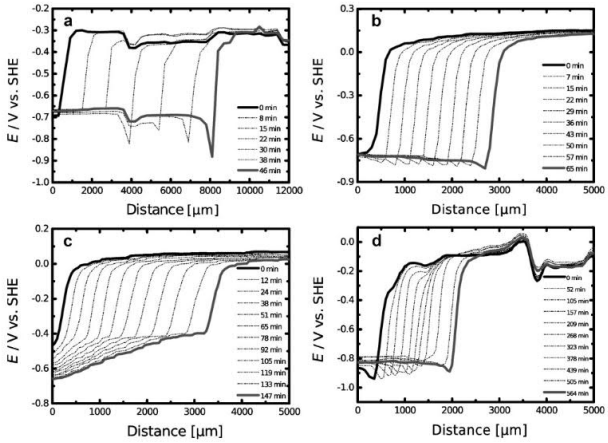

Figure 2. SKP delamination profiles in humid air on PVB coated zinc (a) without any artificial oxide, (b) with ZnO twin plates, (c) with ZnO rods, and (d) with ZnO spheres

It is evident from Fig. 3 that progress of the delamination front is by far fastest for PVB on zinc without particles, where a delamination rate of ~11 mm/h is observed. The statistical error for all delamination rates reported in this work, including those on the surface with spherical, twin-plate-shaped, and rod-like particle, is 0.05 mm/h, which was obtained as the SD from three samples treated according to the same scheme. The actual uncertainty is likely to be higher, due to systematic errors and uncertainties in readout and sample preparation. While on the modified surfaces, thick layers of zinc oxide microstructures are present, the untreated zinc possesses only its native oxide layer. The observed strong reduction in delamination rate may

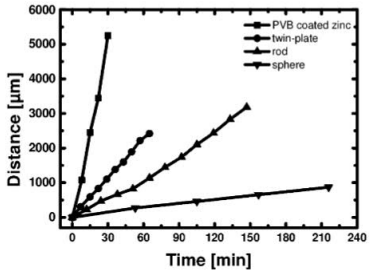

Figure 3. Progress of the delamination front with time on differently structured surfaces. The slope of the linear fit to the points is the delamination rate

therefore have two origins. First, it may be related to an inhibition of the oxygen reduction reaction (ORR), as was observed after deposition of simonkolleite corrosion products on zinc [39]. Second, the deposited thick layer may protect longer zinc against dissolution, as the zinc oxide layer needs more time to dissolve under the alkaline conditions present after the delamination front compared to the thin native oxide. It is also important to note that during delamination process, reprecipitation, i.e. formation of zinc hydroxide from solution, takes place, which does not passivate the surface due to porous nature of the film formed [46,47].

Now, focusing on the delamination rates of the different zinc oxide-modified samples, namely containing zinc oxide spheres, rods, or twin-plates (Fig. 3), a clear difference between the different surface morphologies is observed. Delamination velocity of cathodic delamination is slowest in the case of deposited zinc oxide spheres, where it is ~0.2 mm/h, while it is fastest on zinc oxide twin-plate samples with ~2 mm/h. Rod-shaped structures show a rate of ~1 mm/h, i.e. in between spheres and twin plates.

For all three different morphologies, a reduction in the ORR activity is expected. Previous studies have shown that zinc oxide dissolution in an alkaline medium (as present under the conditions here in the passing of the delamination front) takes place at crystal step edges [40,48]. Macroscopically, a sphere has a smooth surface, without sharp edges and corners, which may explain the particularly low delamination rates on surfaces covered with spherical particles. Sharp corners are present in the case of rod-like and twin-plate structures. From the crystal structure of zinc oxide, one expects, after typical *c*-axis growth, the top and bottom of the cylinder to be terminated with a polar (0001)

or (000-1) surface, while the sides should be terminated with the lower energy non-polar [e.g., (1010) or (1011)] surface [41,45]. Consequently, twin plates are expected to have the highest fraction of polar surfaces, while this fraction is reduced in rod-shaped crystals. This difference is reflected in the faster dissolution of the twin-plate covered zinc compared to rod-covered zinc. The actual surface termination of the spherical particles is not intuitively obvious. Attempts to conclude the orientation of the surfaces from the XRD data shown in Fig. 1 may be misleading, as this shows the predominant crystal growth direction perpendicular to the surface, which is not necessarily the decisive growth direction. As the surface of a spherical particle is, however, homogenous, one should expect a non-polar surface with defects to adjust to the curvature. These defects are, however, obviously not those needed to facilitate dissolution. Kinks and edges on the other hand must be present on the twin plates and rod, and are obvious sites for start of oxide dissolution under basic pH. Therefore, the cathodic delamination process is accelerated on zinc oxide rods and twin-plates in comparison to spheres.

A second factor which needs to be considered is the availability of surface regions which are not covered by µm thick oxides. In these regions, oxygen has easy access to the metal, and the rate of the ORR is therefore faster. For a detailed analysis of the importance of this effect, however, a detailed study of the interface between oxide and metal is needed, which is rather difficult to perform.

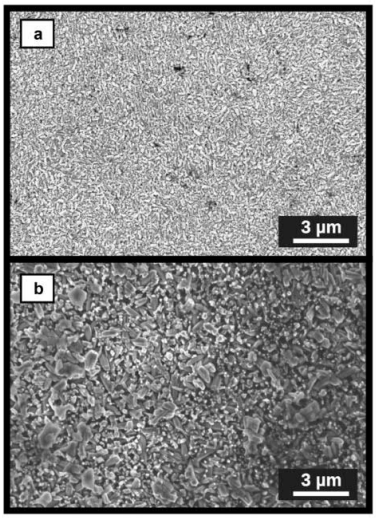

Figure 4. SEM micrographs after the delamination of PVB from (a) ZnO twin-plate-covered surface and (b) ZnO rod-covered surface

An inspection of the surfaces after delamination also points to the importance of the oxide dissolution. SEM images after the cathodic delamination experiment are shown in Fig. 4. All the twin-plate structures have been dissolved. Rod-like structures have also been destroyed, however, the final morphologies resemble rods. Comparison to the initial morphologies (Fig. 1) points to the importance of oxide dissolution in determining the rate of cathodic delamination.

Two more potential factors of influence on the delamination rate, though through evidence here considered as not decisive, shall be discussed, (a) the adsorption of the capping agent and (b) the effect of the overall amount of zinc oxide in the interface, i.e., the layer thickness. Organic capping agents have been used for the synthesis of spherical and twin-plate-shaped structures, while rod-shaped structures have been prepared without capping agents. As the rate increases in the sequence sphere < rod < twin-plate, i.e., the delamination rate for the capping agent free system is in between those with capping agents, there is indirect evidence that the adsorption of residual capping agent in the delamination experiments is not decisively determining the delamination rate. If, on the other hand, the dissolution of zinc oxide is decisive, the total amount of zinc oxide in the interfacial region may contribute to the observed differences in delamination kinetics. On the basis of XRD data shown in Fig. 1, it can be concluded that the overall layer thickness of zinc oxide is lowest in case of the rod-shaped structures. In the case of these structures, the ratio between the strongest diffraction peaks from the substrate zinc to the strongest diffraction peak of zinc oxide is highest, indicating a lower layer thickness than obtained for twin-plate-shaped and spherical particles. On the basis of the sequence of delamination rates observed here it can be again inferred that the total layer thickness cannot be the only determining factor, but that indeed the morphology plays a central role.

4 Conclusions

The deposition of zinc oxide on zinc substantially decreases the delamination rate of polymer coatings on top. The morphology of zinc oxide plays a crucial role in the determination of the delamination kinetics, with a factor of 10 between the lowest (spherical particle) and highest (twin-plate-shaped particle) delamination rates. A comparison of the surface morphologies before and after the delamination experiments shows that dissolution of the oxide in the interfacial region occurs. The kinetics of delamination is likely determined by the nature of the dominating surface termination of zinc oxide. These results suggest that a careful control over surface morphologies in a pretreatment-like process offers the chance to significantly increase resistance of polymer-coated galvanized steel towards cathodic delamination.

Acknowledgments: *D.I.* gratefully acknowledges the International Max Planck Research School for Surface and Interface Engineering in Advanced Materials (IMPRS-SurMat) for a scholarship. All authors thank Prof. *Stratmann* for his continuous support.

5 References

[1] A. Nazarov, D. Thierry, *Electrochim. Acta* **2007**, *52*, 7689.
[2] J. Wielant, R. Posner, R. Hausbrand, G. Grundmeier, H. Terryn, *Corros. Sci.* **2009**, *51*, 1664.
[3] R. Posner, M. Marazita, S. Amthor, K. J. Roschmann, G. Grundmeier, *Corros. Sci.* **2010**, *52*, 754.
[4] P. A. Steward, J. Hearn, M. C. Wilkinson, *Adv. Colloid Interface Sci.* **2000**, *86*, 195.
[5] G. Grundmeier, M. Stratmann, *Mater. Corros.* **1998**, *49*, 150.
[6] D. E. Tallman, G. Spinks, A. Dominis, G. G. Wallace, *J. Solid State Electrochem.* **2002**, *6*, 73.
[7] G. Grundmeier, C. Reinartz, M. Rohwerder, M. Stratmann, *Electrochim. Acta* **1998**, *43*, 165.
[8] J. L. Fang, Y. Li, X. R. Ye, Z. W. Wang, Q. Liu, *Corrosion (Houston, TX, U.S.)* **1993**, *49*, 266.
[9] A. Vimalanandan, L.-P. Lv, T. H. Tran, K. Landfester, D. Crespy, M. Rohwerder, *Adv. Mater.* **2013**, *25*, 6980.
[10] C. S. Che, J. T. Lu, G. Kong, Q. Y. Xu, *Acta Metall. Sin. (Engl. Lett.)* **2009**, *22*, 138.
[11] X. G. Zhang, *Corrosion and Electrochemistry of Zinc*, Plenum Press, New York, London **1996**.
[12] H. Leidheiser, *Corrosion (Houston, TX, U.S.)* **1982**, *38*, 374.
[13] S. Maeda, *Prog. Org. Coat.* **1996**, *28*, 227.
[14] W. Fürbeth, M. Stratmann, *Corros. Sci.* **2001**, *43*, 207.
[15] R. Posner, K. Wapner, S. Amthor, K. J. Roschmann, G. Grundmeier, *Corros. Sci.* **2010**, *52*, 37.
[16] P. Taheri, T. Wielant, T. Hauffman, J. R. Flores, F. Hannour, J. H. W. de Wit, J. M. C. Mol, H. Terryn, *Electrochim. Acta* **2011**, *56*, 1904.
[17] P. Thissen, J. Wielant, M. Koyer, S. Toews, G. Grundmeier, *Surf. Coat. Technol.* **2010**, *204*, 3578.
[18] C. Noguera, *J. Adhes.* **1996**, *57*, 91.
[19] P. Taheri, T. Hauffman, J. M. C. Mol, J. R. Flores, F. Hannour, J. H. W. de Wit, H. Terryn, *J. Phys. Chem. C* **2011**, *115*, 17054.
[20] J. Zuo, A. Erbe, *Phys. Chem. Chem. Phys.* **2010**, *12*, 11467.
[21] Y. Chen, P. Schneider, B. J. Liu, S. Borodin, B. Ren, A. Erbe, *Phys. Chem. Chem. Phys.* **2013**, *15*, 9812.
[22] Y. Chen, P. Schneider, A. Erbe, *Phys. Status Solidi A* **2012**, *209*, 846.
[23] Y. Chen, A. Erbe, *Surf. Sci.* **2013**, *607*, 39.
[24] W. I. Park, G. C. Yi, *Adv. Mater.* **2004**, *16*, 87.
[25] M. Law, L. E. Greene, J. C. Johnson, R. Saykally, P. D. Yang, *Nat. Mater.* **2005**, *4*, 455.
[26] S. Baruah, R. F. Rafique, J. Dutta, *NANO* **2008**, *3*, 399.
[27] T. Y. Wei, P. H. Yeh, S. Y. Lu, Z. Lin-Wang, *J. Am. Chem. Soc.* **2009**, *131*, 17690.
[28] V. H. Grassian, *J. Phys. Chem. C* **2008**, *112*, 18303.
[29] I. A. Mudunkotuwa, T. Rupasinghe, C. M. Wu, V. H. Grassian, *Langmuir* **2012**, *28*, 396.
[30] H. D. Yu, Z. P. Zhang, M. Y. Han, X. T. Hao, F. R. Zhu, *J. Am. Chem. Soc.* **2005**, *127*, 2378.
[31] Z. W. Pan, Z. R. Dai, Z. L. Wang, *Science* **2001**, *291*, 1947.
[32] R. S. Moirangthem, P. J. Cheng, P. C. H. Chien, B. T. H. Ngo, S. W. Chang, C. H. Tien, Y. C. Chang, *Opt. Express* **2013**, *21*, 3010.
[33] D. B. Wang, C. X. Song, Z. S. Hue, *Cryst. Res. Technol.* **2008**, *43*, 55.
[34] T. M. Shang, J. H. Sun, Q. F. Zhou, M. Y. Guan, *Cryst. Res. Technol.* **2007**, *42*, 1002.
[35] Y. H. Tseng, M. H. Liu, Y. W. Kuo, P. L. Chen, C. T. Chen, Y. F. Chen, C. Y. Mou, *Chem. Commun.* **2012**, *48*, 3215.
[36] F. H. Zhao, X. Y. Li, J. G. Zheng, X. F. Yang, F. L. Zhao, K. S. Wong, J. Wang, W. J. Lin, M. M. Wu, Q. Su, *Chem. Mater.* **2008**, *20*, 1197.
[37] R. Krieg, M. Rohwerder, S. Evers, B. Schuhmacher, J. Schauer-Pass, *Corros. Sci.* **2012**, *65*, 119.
[38] P. Volovitch, T. N. Vu, C. Allely, A. Abdel Aal, K. Ogle, *Corros. Sci.* **2011**, *53*, 2437.
[39] J. D. Yoo, P. Volovitch, A. Abdel Aal, C. Allely, K. Ogle, *Corros. Sci.* **2013**, *70*, 1.
[40] M. Valtiner, X. Torrelles, A. Pareek, S. Borodin, H. Gies, G. Grundmeier, *J. Phys. Chem. C* **2010**, *114*, 15440.
[41] L. Vayssieres, *Adv. Mater.* **2003**, *15*, 464.
[42] Y. H. Tseng, H. Y. Lin, M. H. Liu, Y. F. Chen, C. Y. Mou, *J. Phys. Chem. C* **2009**, *113*, 18053.
[43] C. L. Kuo, T. J. Kuo, M. H. Huang, *J. Phys. Chem. B* **2005**, *109*, 20115.
[44] R. S. Moirangthem, A. Erbe, *Appl. Phys. Lett.* **2013**, *103*, 051108.
[45] C. Wöll, *Prog. Surf. Sci.* **2007**, *82*, 55.
[46] B. E. Conway, D. C. W. Kannangara, *J. Electrochem. Soc.* **1987**, *134*, 906.
[47] M. Mokaddem, P. Volovitch, K. Ogle, *Electrochim. Acta* **2010**, *55*, 7867.
[48] N. J. Nicholas, W. Ducker, G. V. Franks, *Langmuir* **2012**, *28*, 5633.

(Received: November 26, 2013) W7533
(Accepted: December 19, 2013)

